Characteristics of Pattern Formation and Evolution in Approximations of *Physarum* Transport Networks

Jeff Jones*
University of the West of England

Keywords
Pattern formation, transport networks, *Physarum polycephalum*, reaction-diffusion, emergent behavior

Abstract Most studies of pattern formation place particular emphasis on its role in the development of complex multicellular body plans. In simpler organisms, however, pattern formation is intrinsic to growth *and* behavior. Inspired by one such organism, the true slime mold *Physarum polycephalum*, we present examples of complex emergent pattern formation and evolution formed by a population of simple particle-like agents. Using simple local behaviors based on chemotaxis, the mobile agent population spontaneously forms complex and dynamic transport networks. By adjusting simple model parameters, maps of characteristic patterning are obtained. Certain areas of the parameter mapping yield particularly complex long term behaviors, including the circular contraction of network lacunae and bifurcation of network paths to maintain network connectivity. We demonstrate the formation of irregular spots and labyrinthine and reticulated patterns by chemoattraction. Other Turing-like patterning schemes were obtained by using chemorepulsion behaviors, including the self-organization of regular periodic arrays of spots, and striped patterns. We show that complex pattern types can be produced without resorting to the hierarchical coupling of reaction-diffusion mechanisms. We also present network behaviors arising from simple pre-patterning cues, giving simple examples of how the emergent pattern formation processes evolve into networks with functional and quasi-physical properties including tensionlike effects, network minimization behavior, and repair to network damage. The results are interpreted in relation to classical theories of biological pattern formation in natural systems, and we suggest mechanisms by which emergent pattern formation processes may be used as a method for spatially represented unconventional computation.

1 Introduction—Pattern Formation, Background, Mechanisms, and Modeling

Pattern formation mechanisms play a critical role in organism development and survival, from embryonic development to the growth and maintenance of the organism. The central question (still, to a great extent, unanswered) posed for all multicellular organisms is: How do the complex multicellular patterning,

* Centre for Unconventional Computing, University of the West of England, Coldharbour Lane, Bristol, BS16 1QY, UK. E-mail: jeff.jones@uwe.ac.uk

differentiation, and functional abilities of a complete organism arise from a single cell? The patterning completed at the end of embryonic development is manifold: Limb positioning, formation of organ systems, completion of vascular and respiratory systems, and skin or coat patterning are just a few notable examples. Many pattern formation mechanisms are under genetic control—their temporal and spatial development apparently guided by expression of genes at critical times and locations. Other patterning mechanisms are thought to be under epigenetic influences, occurring spontaneously with only simple pre-patterning cues, or without *any* prior pre-patterning.

The question of how spatial patterns may arise from a homogeneous initial state was initially addressed by Turing, who considered the interactions of two hypothetical chemicals [51]. The method relied on the autocatalytic production of an activator chemical, which enhanced the production of a second chemical, which in turn inhibited the formation of the activator chemical. Critically, the inhibitor diffused more quickly than the activator, and a pattern of local activation (reaction) and lateral inhibition (diffusion) was produced. Variations in the parameters of the differential equations describing the interactions of the chemicals (which Turing called *morphogens*) produced instabilities in the concentration profiles of the reactants. By interpreting the concentrations of the two chemicals as, for example, different colors, characteristic patterns of spots or stripes are formed. The reaction-diffusion approach has been the dominant theoretical model of pattern formation, and the mechanisms have been used for explanations of both gross body plan and specialized organ development [18, 28] and coat and skin patterns [29, 35].

Many variations of Turing's original two-morphogen method have been developed in attempts to develop more complex patterning. These include the effects of different boundary conditions and extra sources and sinks of chemical stimuli [30], and the coupling of different reaction-diffusion (RD) processes. For example, the output of one patterning process P-A may be used as the input pattern (concentration profile) for a separate process P-B. The combination of different simple patterning processes generates even more complex patterns [52].

Although RD approaches are capable of producing complex patterning, there are still a number of questions as to whether they are actually responsible for pattern formation in living systems. The search for actual morphogen chemicals has yet to reveal definitive results (although there are some notable candidates, such as retinoic acid [34]). It is only relatively recently that Turing-like RD patterns have been observed in chemical systems [14, 40]. Significantly, the RD systems appear to be sensitive to perturbations, which cannot be the case in, for example, embryonic development.

It is also well known that a number of other mechanisms are able to generate complex patterning. Mechanical models have been suggested as pattern formation mechanisms—in these systems the substrate is deformed in some way (for example by cellular traction forces) so as to provide local autocatalytic stimuli to attract local cells and initiate patterning [36]. Alternatively, cellular models exist that utilize purely chemotactic stimuli to allow cells to migrate toward concentration gradients and initiate patterning [33, 42]. More recently, combinations of these methods have been used: the mechanochemical approaches [32, 48].

Oster suggested that it is possible to classify all of the above mechanisms as lateral inhibition based. In his classification [39] all of the previously mentioned methods utilize the phenomena of local attraction and long-range inhibition (LALI). Although the local activation mechanisms all utilize some form of autocatalytic behavior, the inhibition can take very different forms: There may be direct lateral inhibition (for example, by neural inhibition), direct inhibition by a diffusing inhibitor chemical (as in Turing-type RD), or indirect inhibition by substrate depletion or a movement away from a local "zone of influence."

The above approaches are inspired by fine-grained chemical, substrate, and cellular interactions. They are most commonly modeled, however, by continuum-based mathematical models. Bonabeau suggested that agent-based (or "individual-based") modeling may be more suitable for modeling those systems where low-level interactions produce emergent global behaviors [12]. Pattern formation mechanisms in nature are usually composed of very large populations of discrete, relatively independent entities and can be seen in both living and nonliving systems at very different spatial and temporal scales. In nonliving physical systems Turing-like patterning has been observed in vertically oscillated granular

media [9]. At larger spatial and time scales complex patterning has been observed in sorted stone ground in climatic regions where freeze-thaw cycles regularly occur (see [27] for a persuasive model).

In living systems complex patterning is observed in many instances where large colonies of individuals exist, including aggregation in the cellular slime mold *Dictyostelium discoideum* [53], growth patterns in bacterial colonies [8], social insect movement patterns [15], and nest structures [11]. Complex patterning continues as the size of the individual increases: Flocking patterns of birds [41], pedestrian movement [13], and traffic flow [20] are all well-studied examples. Some of these pattern formation mechanisms have certain features in common: The patterning is an emergent phenomenon, qualitatively different from, and not specified by, the individual behaviors. The patterns are often composed of the "actors" themselves [10] from the "bottom up," and the patterns formed may be used for transport of substances within the organism structure [7, 23]. Finally, the patterns formed are often dynamic, adaptable in response to changing environmental conditions (such as nutrient availability), and resilient to external damage. These examples illustrate how patterning in populations of many entities shares features with classical pattern formation during development, albeit on very different spatial and temporal scales.

One particular organism, the true slime mold *Physarum polycephalum*, exhibits a very wide repertoire of pattern formation behaviors used for growth, movement, food foraging, nutrient transport, hazard avoidance, and shape maintenance. *Physarum* is a unicellular, multinucleate protist organism belonging to the phylum Myxomycota (the true, or plasmodial, slime molds, as opposed to the Dictyosteliomycota, or cellular slime molds). Although *Physarum* has a very complex life cycle, its plasmodium stage of vegetative growth exhibits the most complex and well-studied behaviors.

The plasmodium of *Physarum* is a membrane-bound syncytium of nuclei within a cytoplasm composed of a complex gel-sol network. The gel phase is composed of a spongelike matrix of contractile actin and myosin fibers through which the protoplasmic sol flows. Local oscillations in the thickness of the plasmodium spontaneously appear with approximately 2-min duration [44]. The spatial and temporal organization of the oscillations has been shown to be extremely complex [45] and affects the internal movement of sol through the network by assembly and disassembly of the local actin-myosin structures. The protoplasm moves backward and forward within the plasmodium in a characteristic manner known as shuttle-streaming.

The plasmodium is able to sense local concentration gradients, and the presence of nutrient gradients appears to alter the structure of external membrane areas. The softening of the outer membrane causes a flux of protoplasm in the general direction of the gradient in response to internal pressure changes caused by the local thickness oscillations (Figure 1, left). The strong coupling between membrane contraction and streaming movement is caused by the incompressibility of the fluid, requiring a constant

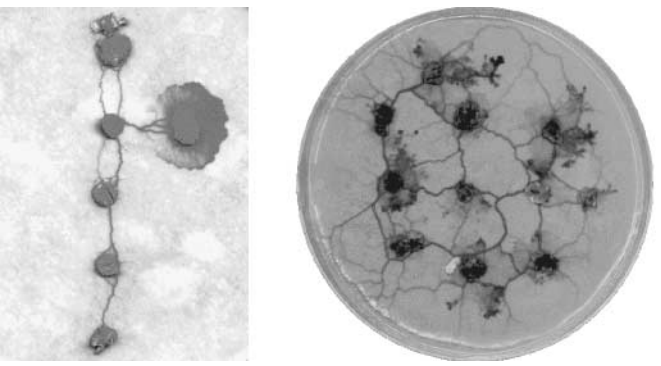

Figure 1. Plasmodium growth and protoplasmic vein formation in *Physarum polycephalum*. Left: illustration of protoplasmic tube network (vertical connections between oat flakes) and active plasmodium growth front forming the horizontal connection. Right: formation of protoplasmic tube network within the plasmodium connecting nutrient sources (oat flakes). (Images courtesy of Andrew Adamatzky.)

volume—the weakening of the membrane provides an outlet for the pressure. When the plasmodium has located and engulfed nearby food sources, protoplasmic veins appear within the plasmodium, connecting the food sources (Figure 1, right). The veins transport protoplasm among the distributed extremes of the organism.

The relative simplicity of the cell and the distributed nature of its control system make *Physarum* a suitable subject for research into distributed computation substrates. In recent years there has been a wealth of research into its computational abilities, prompted by Nakagaki et al., who reported the ability of *Physarum* to solve path planning problems [38]. Subsequent research has confirmed this and broadened the range of abilities to spatial representations of various graph problems [3, 37, 43] and combinatorial optimization problems [6], to construction of logic gates [49] and logical machines [2, 5], and to the achievement distributed robotic control [50], robotic manipulation [4], and robotic amoebic movement [22].

From a pattern formation perspective, *Physarum* can be interpreted as a complex mechanism of planar[1] pattern formation based upon the two requirements of efficiency in foraging behavior (searching of a maximal area) and efficiency in nutrient transport (minimal transport distance and fault tolerance). The mechanisms used to fulfil these requirements are growth, movement, and area reduction. During the growth-and-foraging stage the plasmodium exhibits a default, broadly reticulated outward growth pattern—albeit one that is influenced by substrate and gradient quality [46]. Once nutrients have been located, the topology of the pattern is influenced by the nutrient distribution—the connectivity patterns (the protoplasmic tube network) evolve to achieve a compromise between minimal transport costs and fault tolerance. Since the plasmodium obviously cannot have any global knowledge about the initial or optimal topology, the network must evolve by physical forces acting on the protoplasmic transport.

Tero et al. have suggested that protoplasmic flux through the network veins may be the physical basis for evolution of the transport network: Given sol flux through two paths, the shorter path will receive more. If there is an autocatalytic mechanism to reward veins with greater flux (by thickening/widening them) and to apply a cost to veins with less flux (the veins become thinner), shorter veins begin to predominate as the network evolves. This approach was used for the mathematical model of *Physarum* network behavior to solve path planning problems [47]. This method also concurs with the previously mentioned formulation of Oster for pattern formation by local activation (strengthening of shorter tubes) and lateral inhibition (weakening of longer ones). The starting point for the model of Tero et al. is a randomly connected protoplasmic tube network, surrounding a number of food sources (network nodes), which act as sources and sinks of flux. By beginning with a complete network, this method, although successful in generating impressive solutions to network problems, sidesteps the issue of initial network formation.

Gunji et al. introduced a cellular automaton (CA) model that considered both plasmodial growth and amoeboid movement [19]. Their model placed importance on the transformation between hardness and softness at the membrane and the internal transport of material from the membrane, resulting in movement and network adaptation. The model was also able to approximate instances of maze path planning and coarse approximations of the Steiner tree problem.

Takamatsu et al.'s hexagonal CA [46] is an early-stage model initially concerned with mimicking the growth patterns displayed under differing nutrient concentrations and substrate hardnesses. The patterns reflect experimental results well, but do not (at least at this stage—oscillatory behavior is in development) show morphological adaptation as the plasmodium grows. Hickey and Noriega adapted a classical ant colony optimization algorithm to modify a decision tree in their representation of *Physarum* behavior in a simple path planning problem [21]. Their algorithm (as with many implementations of ant algorithms) transformed the spatial representation into a graph representation and provided broadly similar results to path optimization by *Physarum*. The growth of a plasmodium from a single node to create a spanning tree to nearby isolated food sources appears similar to the behavior of a neural growth algorithm suggested by Adamatzky [1].

1 *Approximately* planar, since although *Physarum* can grow over any surface, the plasmodium itself typically is very thin and can be treated as a planar sheet.

This article adopts a synthetic multi-agent, chemotaxis-based approach to generate dynamic emergent pattern formation, inspired by the adaptive behavior of *Physarum polycephalum*. We demonstrate spontaneous pattern formation in which the patterns are composed of the flux of agent movement. We present results generated both with and without initial pre-patterning cues and explain the simple mechanisms that generate the complex patterns. The approach is based on cell migration and uses a single synthetic (in silico) chemical. The approach does not require explicit lateral inhibition, and it is not necessary to resort to multiple morphogen chemicals or the hierarchical coupling of different RD processes to achieve the wide range of patterns demonstrated. We show that emergent quasi-physical behaviors are responsible for complex network evolution. The local sensory behaviors and mobility of the agent particles in the model described in this article suggest similarities with the ant colony optimization (ACO) approaches introduced by Dorigo (see [17] and [16]). It should be noted, however, that actual implementations of the ACO tend to abstract the spatial environment into a graph representation (as with Hickey and Noriega's approach). Thus, in a typical implementation, there is no actual movement of the agents along paths—deposition is computed as a function of path length, and the graph is updated *as if* a certain number of ants moved along the graph. We would suggest (based on evidence shown in Section 4 of this article) that although the graph representation lends itself more to simple algorithmic implementation on classical computing devices (especially with respect to memory requirements and scheduling), the loss of the spatial domain forfeits some of the richness of possible interactions in systems that have actual propagation of information in the spatial domain.

An outline of the remainder of the article is as follows. In Section 2 the multi-agent framework is introduced, and details of the framework scheduler, population environment, agent morphology, and behavioral algorithm are given. Section 3 illustrates the mechanisms and evolution of the pattern formation process in homogeneous environments (without pre-pattern cues). Beginning with chemoattraction behaviors, we describe the formation of the default emergent transport networks and explain some of the emergent phenomena arising from the network formation. An exploration of possible patterning is shown, describing the effects of sensory parameter mapping and the effects of sensory coupling scale, population density, and diffusion gradient strength. An exploration of pattern formation based on chemorepulsive response to stimuli is also described, generating regularly spaced dissipative patterns. Section 4 illustrates the response of the patterning process to existing pre-pattern stimuli, illustrating how the pre-pattern cues affect the evolution of the transport networks. Two methods of network evolution are demonstrated, based on the random formation of the network condensing around the pre-pattern points, and on the effect of the pre-pattern nodes on a preexisting plasmodial sheet that is gradually reduced (shrinking) in size. The section concludes with an illustration of how the emergent transport networks respond to damage to them. The article concludes with a summary of the pattern formation results, some possible biological correlates of the patterning process, and an assessment of the importance of physical (rather than simply geometric) influences on the network topology. In keeping with some of the recent research inspired by the behaviors of *Physarum*, we suggest how the dynamic transport networks may be harnessed for spatially distributed unconventional computation.

2 A Particle-Based Emergent Pattern Formation Model

The model uses a multi-agent approach that was introduced in [24] as a means of constructing synthetic and bottom-up dynamical transport networks. The agents' habitable environment landscape is specified by a two-dimensional digitized grayscale image, and its bounds are the image width and height. Specific grayscale values may used to denote certain features (habitable areas, obstacle boundaries, food stimuli sources, etc.). A layered approach is used: As well as the data landscape layer where the environment configuration is stored and the agents reside, other data structures, identical in size and corresponding to the coordinate system of the data layer, may be used (Figure 2). These separate layers are used to represent the projection of hazardous stimuli to the population (not described in this article) and to store the chemotactic stimuli that the agents both deposit and follow (the *trail* layer). The majority of this report concentrates on pattern formation without any pre-patterning. Later sections illustrate the network

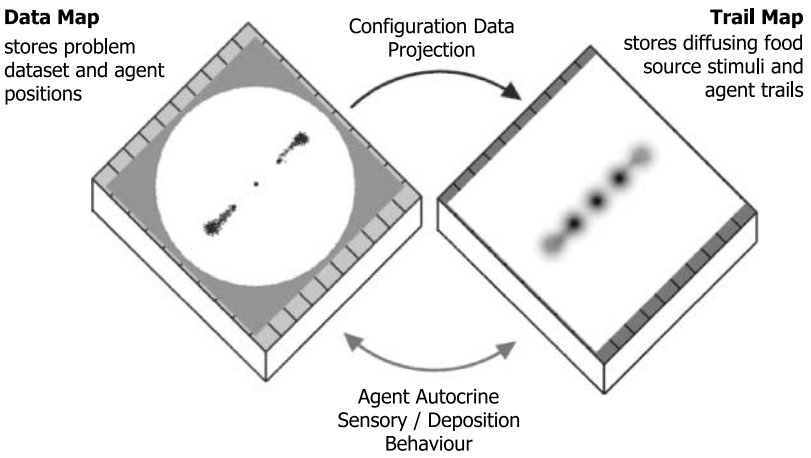

Figure 2. Layered approach of coupled maps used in the framework. Areas on data map indicate pre-patterning stimuli. Such pre-patterning is considered only in the latter sections of this report.

behavior in response to very simple pre-patterning cues: the cues consisting of simple nodes representing preexisting concentration gradients. The dynamic behavior of the population ensures that the networks can respond to any changes in the pre-patterning cues.

The framework is semi-continuous in its approach: Each grid cell can contain only a single agent and is addressed by discrete coordinates. However, the agents also maintain an internal floating point record of their position and direction. The floating point values are rounded to provide the nearest discrete grid cell location. The semi-continuous approach helps overcome the limitations of the discrete connectivity and movement imposed by the discrete architecture. The contents of each layer may also be subject to global environment effects such as evaporation and diffusion, depending on the particular modeling task. The trail data structure is subjected to a simple diffusion operator after every system step (a system step is defined as a sensory sampling of the environment and attempted forward movement for every member of the population). The diffusion operator takes the form of a pseudo-parallel simple mean filter in a 3×3 kernel that is subject to an adjustable decay value to affect chemoattractant persistence.

2.1 Agent Particle Behaviors

The agents follow simple stimulus-response behaviors and are almost particle-like in their simplicity. A single agent represents a hypothetical particle of *Physarum* plasmodium gel-sol structure. When a particle moves, the movement can be said to represent the protoplasmic flux of sol. When a particle is not able to move, it can be said to represent the immobile gel matrix. The general morphology of an agent and its basic underlying algorithm is illustrated in Figure 3. An agent occupies a single discrete location in the environment, corresponding to a single pixel of a digitized image. Each agent is typically initialized at a randomly chosen unoccupied and habitable location and with a random orientation (from 0 to 360 deg, freeing the agent from the restrictive architecture of the underlying discrete image). The agent receives chemotactic sensory stimuli from its environment (chemoattractant levels stored in the trail map) via three forward sensors, and the agent responds to differences in the local environment chemoattractant levels by altering its orientation angle by rotating left or right about its current position. Although specified in nonlinear algorithmic terms (IF-THEN statements), the particle algorithm corresponds simply to cellular behaviors of chemoattraction, orientation, and persistent movement. It should be noted that, in relation to typical agent-based models, the offset sensor distance is large (compared to the agent body size) and would normally correspond to remote sensing behaviors. In this instance, however, the offset distance mimics the overlapping actin-myosin mesh of the plasmodium gel system. The offset sensor design generates significant sensory local coupling between the agent population (the sensory input of one agent can be strongly affected by the actions of nearby agents). Indeed, the strong coupling (minimum distance of 3 pixels

offset) is actually necessary for the complex behaviors to emerge. The cohesion of this aggregate "crowd" is ensured by the fact that there is mutual attraction to the stimuli deposited by the agent population. The population adopts autocrine chemotaxis behaviors (meaning that the agents both secrete and sense approximations of the same chemoattractant, so the actions of the agents can also affect their behavior). One significant simplification with respect to the real organism is that both food sources and the changes in flux of internal protoplasm are represented by the same diffusing chemoattractant substance. The built-in lag between the agent particle movement (a simplistic approximation of actin-myosin contraction movement) and the production and diffusion of protoplasmic sol flux results in complex emergent population behaviors. The agent is forward biased, that is, only the sensors directly in front of the agent's current position are used to influence its behavior, thus ensuring a continuous dynamic.

At each execution step of the scheduler, every agent attempts to move forward one step in the current direction. After every agent has attempted to move, the entire population performs its sensory behavior. If the movement is successful (i.e., if the next site is not occupied) the agent moves to the new site and deposits a constant chemoattractant value. If the movement is not successful, the agent remains in its current position, no chemoattractant is deposited, and a new orientation is randomly selected. Agents are selected from the population randomly in the motor and sensory stages to avoid the possibility of long term bias by sequential ordering. The agent both deposits to and senses from the trail map, resulting in an autocrine mode of stimulus/response. Note that patterning is also possible with a simple passive agent response—where the agent responds to chemoattractant concentration without affecting the chemoattractant levels. The passive approach to particle RD computing is described in [25], and a comparison of the active and passive approaches can be found in [26].

```
[Motor stage]
        - Attempt move forwards in current direction
        - If (moved forwards successfully)
                Deposit trail in new location
        - Else
                Choose random new orientation
[Sensory stage]
        - Sample trail map values
        - if (F > FL) && (F > FR)
                - Stay facing same direction
                - Return
        - Else if (F < FL) && (F < FR)
                Rotate randomly left or right by RA
        - Else if (FL < FR)
                Rotate right by RA
        - Else if (FR < FL)
                Rotate left by RA
        - Else
                Continue facing same direction
```

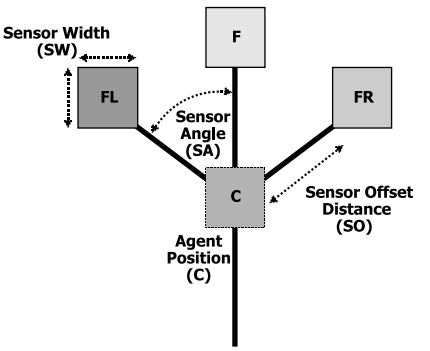

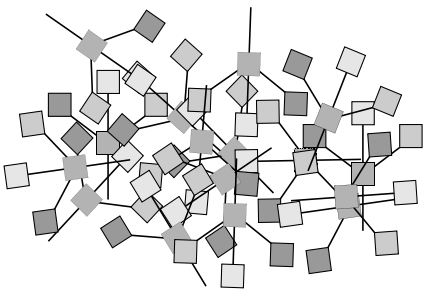

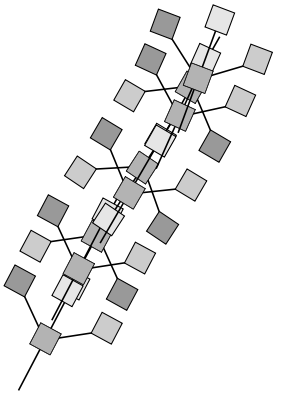

Figure 3. Base agent behavioral algorithm and agent morphology. Top left: Agent motor-sensory algorithm orients agent toward strongest source of chemoattractant gradient and attempts to move forward in current direction. Top right: Individual agent structure showing central position and forward-biased offset sensors. Bottom left: Static collective of agents approximates plasmodium actin-myosin mesh. Bottom right: Mobile stream of agents approximates sol flow within the plasmodium.

Table 1. Model parameters.

Parameter type	Parameter name	Typical values	Description
Framework environment	Image environment	200 × 200 pixels	Environment specified by grayscale image. Specific gray values correspond to properties of environment (obstacles, food sources, start points, exit points).
	%p	3–15	Population as percentage of image area
	diffK	3	Diffusion kernel size
	decayT	0.1	Trail-map chemoattractant diffusion decay factor
	wProj	0.01–0.1	Pre-pattern stimuli projection weight
	Boundary	Periodic	Diffusion and agent environmental boundary conditions
Agent	SA	22.5 or 45 deg	FL and FR sensor angle from forward position
	RA	45 deg	Agent rotation angle
	SO	9 pixels	Sensor offset distance
	SW	1 pixel	Sensor width
	SS	1 pixel per step	Step size—how far agent moves per step
	depT	5	Chemoattractant deposition per step
	pCD	0	Probability of a random change in direction
	sMin	0	Sensitivity threshold

The model contains a number of parameters that govern the multiagent framework as a whole, and the agent behaviors in particular, as listed in Table 1. Although there are a large number of parameters in the table, there are only three main agent parameters that significantly affect patterning (SA, RA, and SO) and two framework parameters with significant effects (%p and decayT).

The parameter values were the same for all of the experiments documented below, except where noted. Two different methods were used to visualize the results. The first method simply places a dark-colored dot to indicate the position of each agent. Alternatively, the values in the diffusing trail map (the chemoattractant levels) can be used to indirectly infer the positions of the agents. The increasing trail-map values are shown as darker areas on the images. Images are taken at notable times during the evolution of the network patterns. Advantages in using the trail-map visualizations are that the diffusion boundaries of the trail networks can be seen, and the flux of trail levels can be visualized. Due to the complexity of the long-term behavior of the networks, the reader is also encouraged to refer to the supplementary video recordings, where noted, which illustrate the dynamic evolution of the system. The video recordings and larger example images of patterning parameterization can be found at http://uncomp.uwe.ac.uk/jeff/pattern_formation_supplementary.htm. Video recordings are referred to below with names beginning "VR F".

3 Spontaneous Pattern Formation without Pre-pattern Cues

Experiments were carried out using the default parameters described in Table 1. After initialization, the randomly distributed agent population spontaneously forms network trails; see Figure 4 and VR F4a–d.

The spatial patterns are composed of the bidirectional flow of agents. The network forms because agents are attracted to the strongest local source of chemoattractant. Individual agents also secrete chemoattractant when they move forward successfully. This behavior ensures that nearby agents are attracted to the sources of chemoattractant and a positive feedback loop is formed. The steep gradient strongly maintains agent flow within the boundaries, and chemoattractant levels quickly fall away from the trail region. Because the agents only deposit chemoattractant after a successful movement and because the agents have a forward-biased sensory apparatus, static clustering of agents is avoided and a dynamic network is formed.

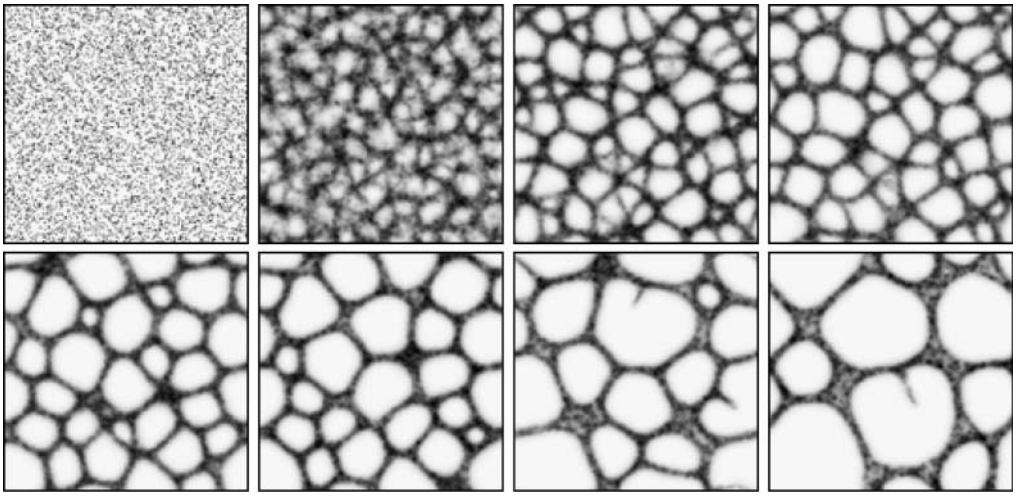

Figure 4. Spontaneous formation and evolution of transport networks. Lattice 200 × 200, %p 15, RA 45, SA 22.5, SO 9. Trail-map patterns, images taken at 2, 22, 99, 175, 367, 512, 1740, and 4151 scheduler steps.

The dynamic nature of the network exhibits complex emergent properties. Smaller cyclic areas of the network gradually contract and disappear. As the smaller cyclic areas disappear, larger lacunae predominate and grow as the smaller regions shrink. Occasionally, however, a bifurcation will appear in one of the network edges, and a new agent-chemoattractant *sprout* will branch out across the dividing space of a single lacuna. This growth sprout is composed of agents moving forward. The direction of growth of the new trail sprout is unpredictable, and when the gap is breached there is a surge of movement as the two moving flows are connected. This surge includes an outflow from the far edge to the moving sprout as agents within the trail at the far edge are attracted to the chemoattractant flow of the sprout.

The result is a dynamic network whose shape is constantly changing but whose composite parts remain the same in number. For the default sensor parameters (RA 45 deg, SA 22.5 deg) the network never stabilizes completely (although *temporarily* stable regimes have been observed, for example in the recordings VR F4e). The complexity of the network evolution is also affected by changes in network structure. For example, the collapse of a cyclic structure by contraction introduces a greater flux of agents into a different part of the network. This greater flux can affect the network flow in local areas, further changing the configuration. A simple relationship is thus formed: The change in network structure (e.g., branching, closing) affects the local agent flux, which in turn affects the network structure, and so on. The dynamic evolution of the network with the default parameters occurs because the rotation angle is significantly greater than the sensor angle. The wide rotation angle places the sensors away from the main gradient stream. If this is coupled with random changes in direction (due to agent-agent collisions), a new bifurcation can become stabilized and reinforced by agent flow.

When both SA and RA are 45 deg, the same initial complex network evolution is observed, but the bifurcation and sprouting of new trails does not persist. In this case the lacunae gradually become larger as the smaller cycles are closed. Eventually a simple network is formed which, when tiled, approximates a regular hexagonal tiling (Figure 5, VR F5a,b).

The networks evolve without any pre-patterning of the environment, and different configurations appear at each run. The shape of the network is influenced by the random initial distribution of agents and the random initial orientation of the agents. The chemoattractant trails that emerge when the agents move break symmetry quickly when, for example, one area by chance accrues more chemoattractant than another. Once agents aggregate in trails, unoccupied areas become more devoid of chemoattractant (as the trails evaporate in general), further amplifying the disparity of (and attraction for) the areas. As in classical approaches to RD pattern formation, there is a reaction component (the deposition of chemoattractant by agents and the orientation toward stronger concentration). There is also a diffusion component (the diffusion of the chemoattractant from the deposition sites). However, unlike classical

morphogen-based models of Turing-type pattern formation, there is no explicit inhibition mechanism present. Note that without the presence of a diffusion mechanism, the patterning would be dependent to a large extent on the initial distribution and orientation of the agents.

As well as the formation of the spatial patterns, the patterns appear to exhibit emergent quasi-mechanical behavior: a contraction effect resembling surface tension. The contraction of cyclic areas both increases local flow (Figure 6) and minimizes network path length, and the stable hexagonal tiling (RA 45, SA 45) is a self-balancing structure. The pattern is stable (although constantly turning over its components) because the interacting trail flows are effectively in competition with each other. The constantly changing network (RA 45, SA 22.5) does not reach minimal configurations as the branching behavior dynamically reconfigures the network—network length is sacrificed for network connectivity.

The mass behavior of the agent population shows collective network formation. When observing a single agent's movement, however, we find that it does not follow the smooth flow that might be expected. The agent is hesitant and moves backward and forward as it progresses along a particular path. To investigate the characteristics of single-agent movement, the movement of a single particle was recorded in a confining environment over the course of 3,000 scheduler steps, and a characteristic result is shown in Figure 7.

The movement is strongly indicative of shuttle streaming flow in *Physarum*, and examples of such movement can be seen in the video recordings VR F6 and VR F7. The changes in direction are due to random deviations in path strength and agent-agent collisions. Although the emergent network area is only a small proportion of the total lattice area, over time the remodeling of the network (with branching behaviors RA 45, SA 22.5) ensures that every part of the lattice is traversed by the population (Figure 8, left, and VR F8a) within 11,000 steps. By tracking the complete record of movement of a single agent in the population (on a smaller lattice for increased speed), a history of movement was collated. It was found that the agent traversed every possible location on the lattice within 475,000 scheduler steps (Figure 8, right, and VR F8b).

3.1 Formation of Planar Structures

It is also possible for the emergent agent networks to form uniform sheetlike structures. Figure 9 shows the evolution of the stable RA 45, SA 45 network without periodic boundary conditions. The agents again coalesce into network trails, and the contraction behavior condenses the network until all interior space is removed and a sheetlike mass remains. This sheet configuration also exhibits

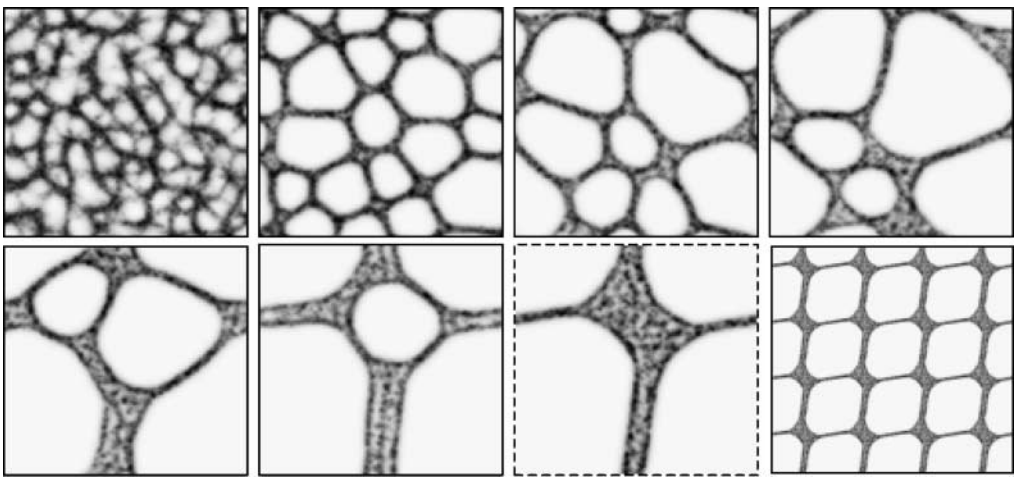

Figure 5. Stable minimizing network approximates hexagonal tiling. Lattice 200 × 200, %p 15, RA 45, SA 45, SO 9. Trail map patterns, images taken at 27, 670, 2364, 4072, 13160, 16850, and 31190 steps. Final image shows approximate hexagonal tiling of stable state image 7 (dashed).

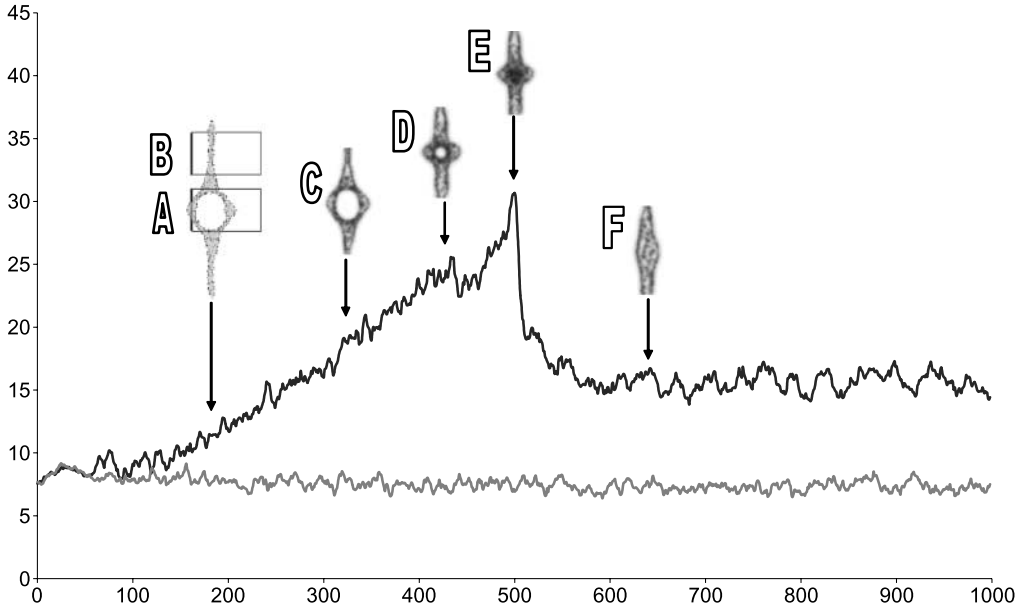

Figure 6. Increase of agent flux as cyclic structures close. *X* axis: scheduler steps; *Y* axis: arbitrary chemoattractant units. The area of the cyclic ring (inset (A) and top plot) increases in the flux of agents as the structure closes. The steep increase (C, D) is also partly because there are two streams in this area. There is a sudden peak (E) when the two paths merge completely. When the contraction is complete, the local flux level reduces (F). The area outside the cyclic structure maintains a relatively stable flux (inset (B) and bottom plot). At later stages, the flux is equalized (not shown) when the bulge in the flow is dissipated along the length of the line.

unusual properties—the sheet itself forms a minimal surface shape, and ripple-like activity can be seen to propagate through the sheet (see VR F9). The sheet also shows relatively stable dissipative *islands* of greater trail flow. The islands reflect areas where a temporary vacancy of agents exists. The number and size of the islands is related to the sensor offset distance (SO) of the agents. When SO

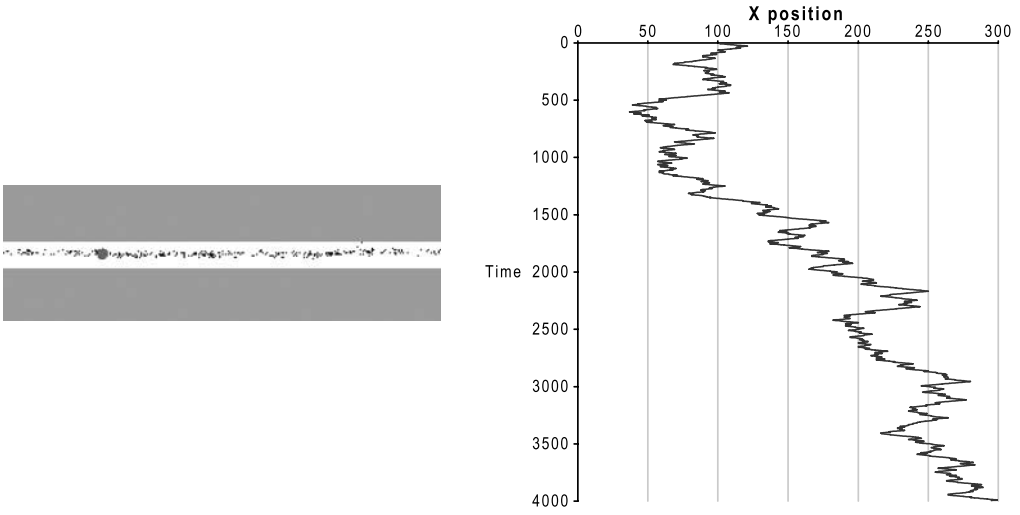

Figure 7. Tracking of single agent particle shows characteristic shuttle streaming movement pattern. Left: Agent particle population confined within narrow corridor with periodic boundary conditions. Larger circle indicates a single tracer agent particle. Right: Plot of agent *X*-coordinate positions over 4,000 scheduler steps. The movement trend to the right side is punctuated by oscillating direction changes, indicative of shuttle streaming.

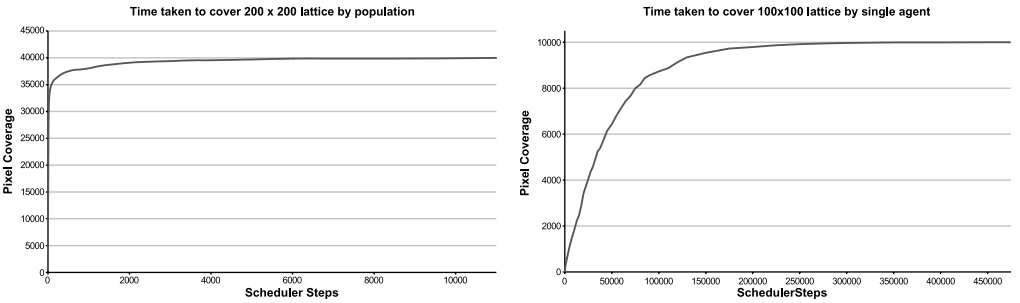

Figure 8. Time taken to traverse entire lattice—population and single agent. Left: Entire population, lattice 200 × 200, %p 10, RA 45, SA 22.5, SO 9. Right: Single agent, lattice 100 × 100, %p 10, RA 45, SA 22.5, SO 5.

increases, the number of vacancy islands decreases and the spacing between them increases (VR F9b). We suggest that the vacancy islands self-assemble based upon agent positions and orientation. The RA 45, SA 22.5 networks also condense when boundary conditions are fixed, but no solid sheetlike mass is formed: The branching activity prevents network condensation into a complete sheet structure (VR F9c).

3.2 Effects of Sensory Scale and Pattern Formation

The parameter SO (the distance between the agent position and the sensors) acts as a scaling factor. Smaller SO values exhibit a more fine-grained structure, while large values show wider patterns and coarser network paths. An example of how SO affects network formation can be seen in Figure 10 for SO distances of 3, 9, 15, and 25 pixels.

The parameter SO affects the scaling of the patterns because the distance from the agent location to the position of the sensors reflects an indirect coupling between separate agents. When SO is small, the agent receives sensory input from the chemical cues of only nearby agents and the coupling is weak. For large SO the increased distance represents a strong coupling between distant agents. The stronger coupling results in coarser patterns with correspondingly large network structures and path thicknesses. In general terms very small sensor offset distances (SO ≈ 3 to 7) result in fine-grained network formation and evolution, while larger offsets result in coarse-grained networks. As the network scale increases, so does the speed of network evolution. The sensor scale may also affect the *type* of pattern formed, due to interplay with population density. At high population densities, there is limited possibility of free agent movement (recall that agents only deposit chemoattractant when a move forward is successful), and, as the sensor offset scale increases, there is a shift in pattern formation from network with lacunae toward striped and spotted patterns (Figure 11). The shift in pattern type at high population densities and large

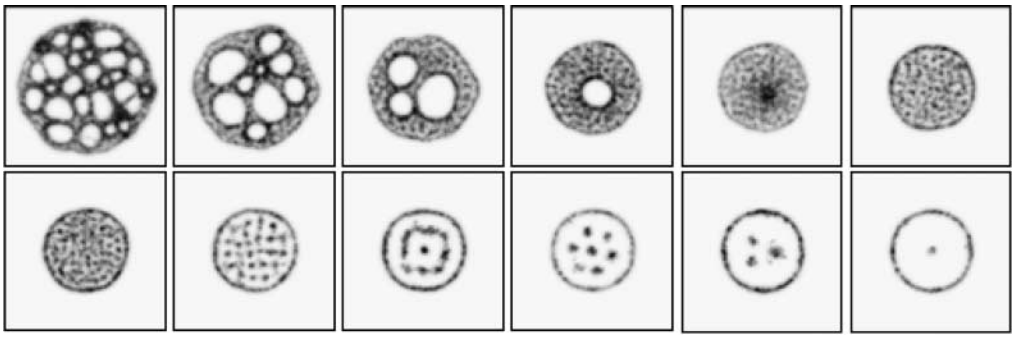

Figure 9. Formation of sheetlike structures from emergent networks and the emergence of dissipative vacancy islands. Top row, left to right: network trail evolution over time: %p = 20 agent trails, RA 45, SA 45. Bottom row, left to right: network trails showing dissipative vacancy island patterns at SO 9, 13, 19, 23, 28, and 38.

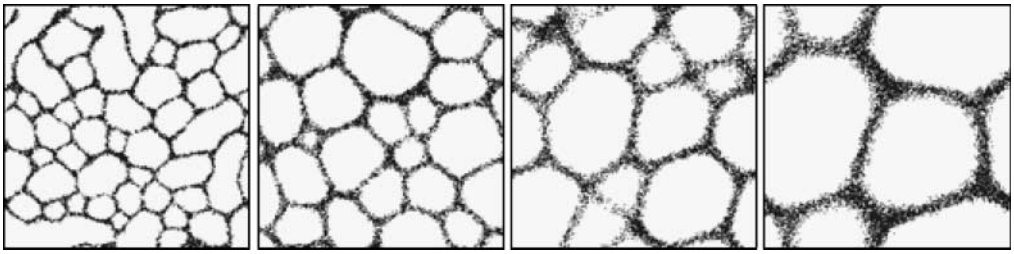

Figure 10. Effect of sensor offset distance (SO) on pattern scale and granularity. Lattice 200 × 200. For all experiments (%p 15, SA 45, RA 45), evolution stopped at 500 steps. Left to right: patterning produced with SO of 3, 9, 15, 25 pixels, particle positions shown.

sensor scales is due to the fact that most agents cannot move. The pattern of spots seen below (for example, at %p 90 and SO 27) is actually produced by the formation of vacancy islands—small regions of vacant space surrounded by areas solidly packed with immobile agent particles. At low %p the patterning is associated with areas of high agent occupancy whereas at high %p the patterning is associated with areas of relatively low occupancy.

3.3 Effect of Diffusion Decay and Population Size

The pattern formation and evolution are also affected by the strength of the diffusion gradient and the initial number of agent particles. Space constraints prevent the illustration of the effects for every RA-SA combination, but Figure 12 shows the effect of increasing population size and decreasing diffusion gradient strength on pattern formation for the RA 45, SA 45 minimization behavior.

Increasing the population size made the network boundaries thicker and reduced the number of lacunae. Increasing the diffusion decay parameter (reducing the strength of the gradient field) produced coarser network edges. With very low decay (very strong gradients) the attraction between the particles was stronger and network connectivity was reduced.

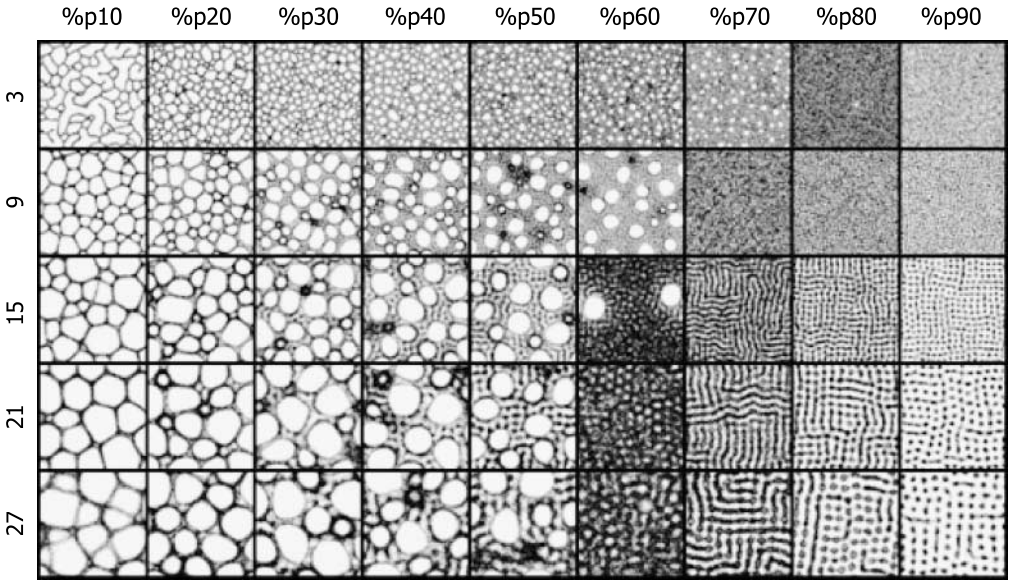

Figure 11. Interaction between population size and sensory scale. Columns: %p. Rows: sensor offset distance. Lattice 300 × 300, RA 45, SA 45, run for 500 steps. Trail patterns shown.

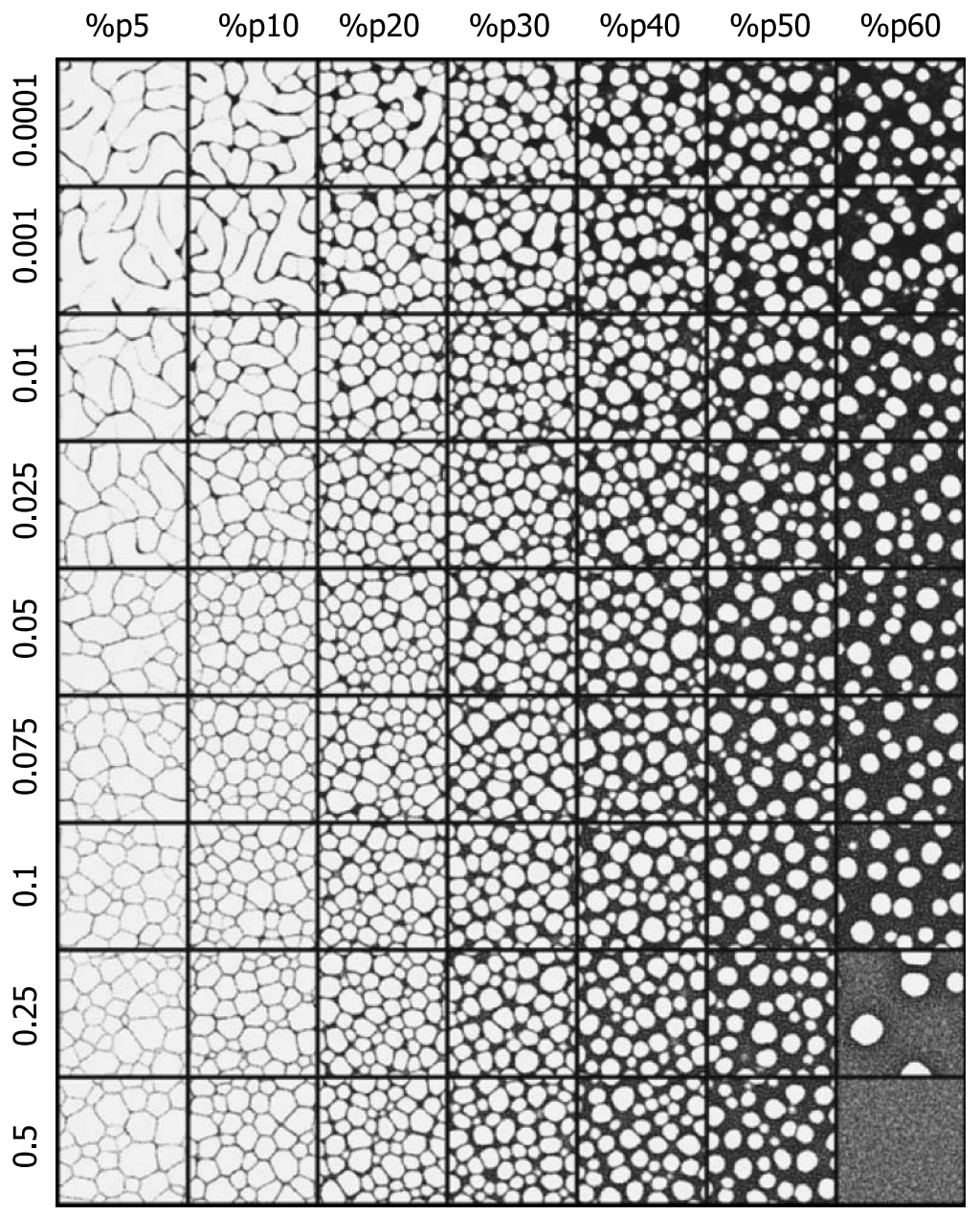

Figure 12. The effect of increasing population size and decreasing diffusion gradients on RA 45, SA 45 patterning. Columns: %p. Rows: diffusion decay strength. Lattice 300 × 300, SO 9, run for 500 steps. Agent particle positions shown.

3.4 Chemoattraction-based Pattern Formation: Parametric Exploration

The previous results exhibit striking differences in pattern evolution by chemoattraction with only small changes in sensory parameters. How prevalent is complex behavior throughout the sensory parameter space? A systematic variation of the sensor angle (SA) and rotation angle (RA) revealed the patterns illustrated in Figure 13, which is a composite image constructed from results at each parameter setting. All experiments were run for 500 steps. Both parameters were monotonically varied from 0 to 180 deg in 22.5-deg increments.

The patterns can be roughly grouped into classes based on their appearance. The patterning ranges from none (or incomplete patterning, especially at 0- and 180-deg SA and 0-deg RA, for obvious reasons), to partial patterning (along the RA 180-deg row), and to clear patterning in the remaining regions. The inner sections of the quadrant show a gradual decrease in connectivity as both RA and SA increase. The patterns can loosely be classed as reticular, labyrinthine, and island-like. Examples from each class are shown in Figure 14. Each column shows four examples from the different pattern classes.

It should be noted that the patterns shown are only brief snapshots at a particular instant in time and the patterns continue to evolve. The course of the evolution may remain disordered (in the case where no patterning was seen), complex (as in RA 45, SA 22.5 with dynamic remodeling), minimizing (as in RA 45, SA 45), or a simplification of the initial patterning (see supplementary video recordings VR F14 for examples of pattern evolution). This differs from *Physarum*, where the patterning is reduced by adhesion of the plasmodium to its substrate (although it would be fairly simple to slow the growth of the model over time to mimic this effect). The patterns formed correspond to changes in cohesion caused by differences in SA and RA. When both parameters are increased together there is a trend from reticular to labyrinthine to island-like patterns, so—in general terms—low values show higher connectivity,

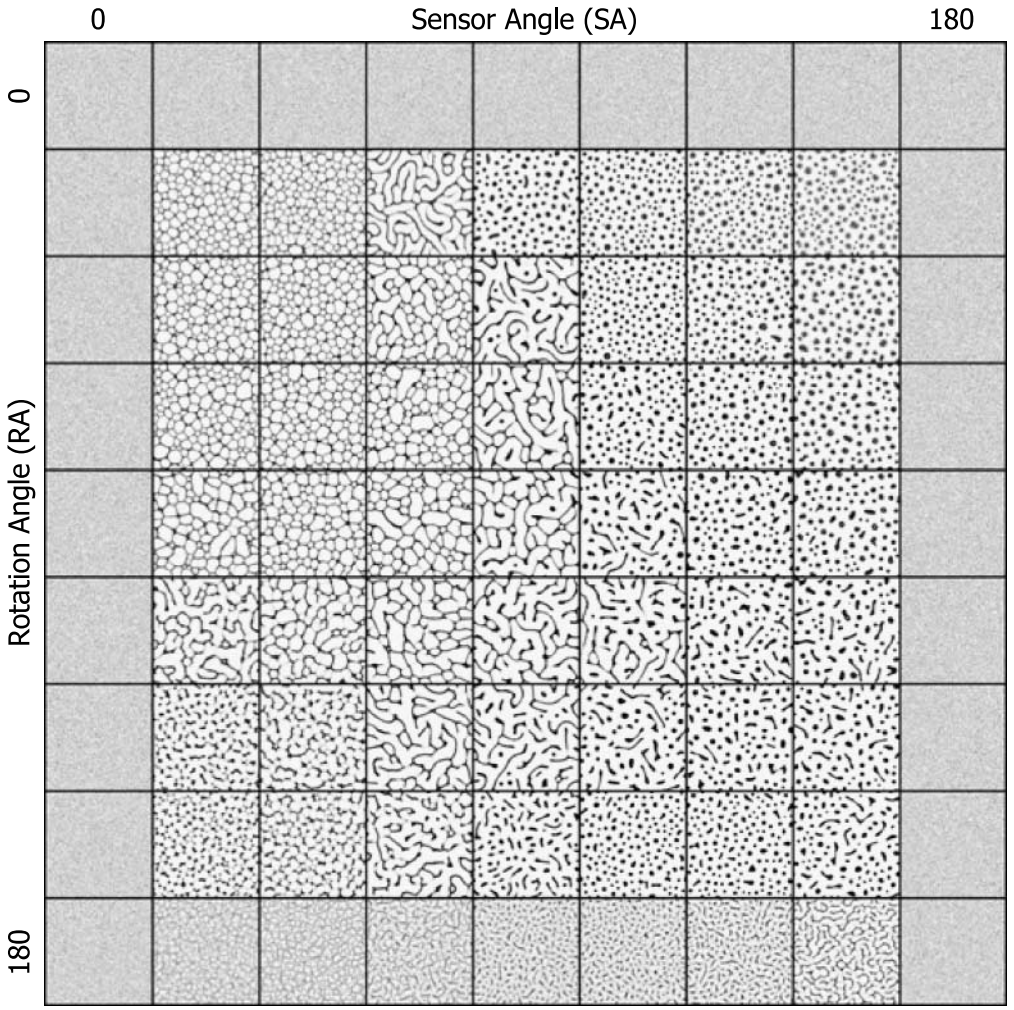

Figure 13. Patterns formed by chemoattraction on varying SA and RA from 0 to 180 deg. 500 × 500 lattice, %p 15, SO 9, run for 500 steps. Agent particle positions shown.

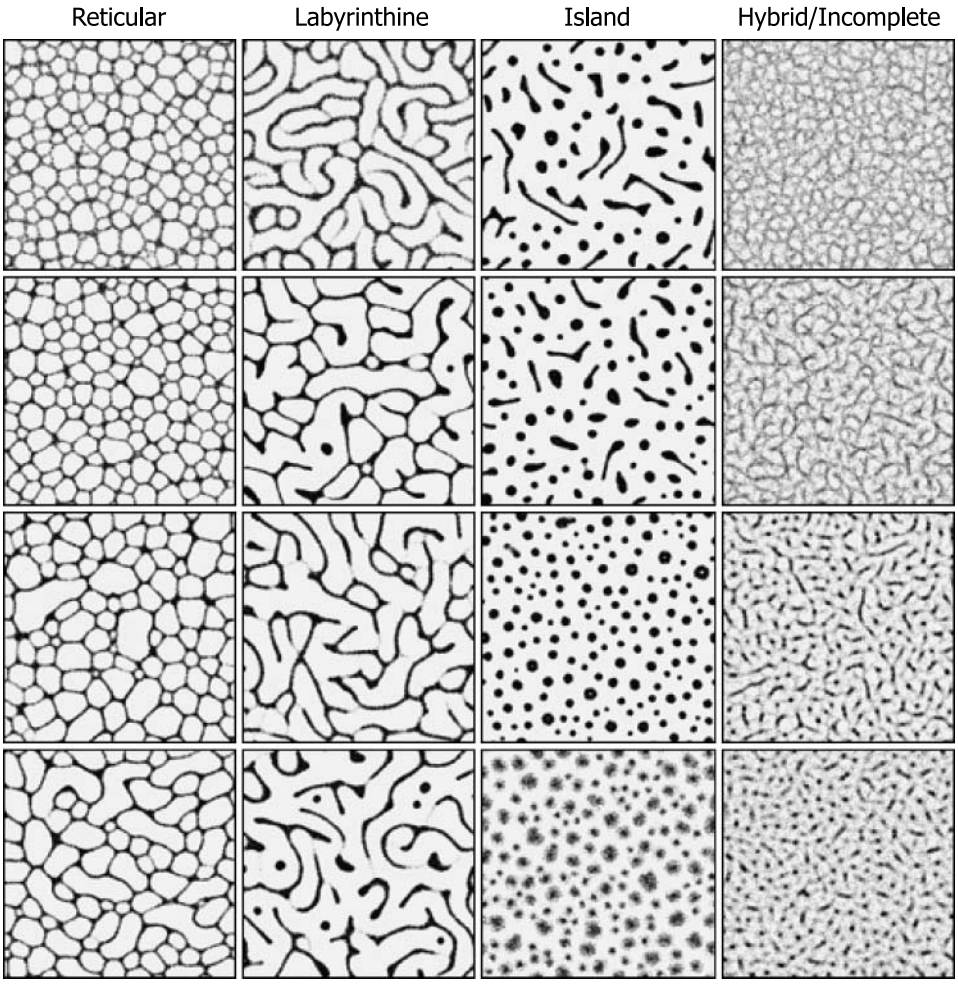

Figure 14. Examples of reticular, labyrinthine, island, and hybrid or incomplete patterns from the parameter space mapping. 500 × 500 lattice, %p 15, SO 9, run for 500 steps. Agent particle positions shown. 1st column: examples of reticular patterns. 2nd column: examples of labyrinthine patterns. 3rd column: examples of island patterns. 4th column: examples of hybrid or incomplete patterning.

whereas higher values result in more isolated patterns. There is also a resemblance between the patterning types in the model system and the patterning of *Physarum* in different parts of its life cycle. When the organism is in a nutrient-rich environment, growth is expansive and highly connected (reticular patterns). When nutrient concentrations are lower, growth is dendritic (labyrinthine patterns). Finally, in more hostile conditions (desiccated and/or exposed to light) there is a switch to isolated dense patterns of the sporelike sclerotium stage. It is interesting to speculate on whether nutrient availability affects the patterning of the organism in a similar way to the model—namely, changing the cohesion of the plasmodium.

3.5 Chemorepulsion-Based Pattern Formation

The attraction of the agents toward the strongest stimuli generated reticular, labyrinthine, and island-like patterning. How would the patterning differ when the agents were instead *repelled* by the chemical deposition that they produced? The patterning in Figure 15, illustrating the sensory parametric variation of SA and RA, shows the emergence of regular structures, reminiscent of classical Turing patterns.

The algorithm for chemorepulsive patterning is conceptually the exact opposite of the algorithm specified in Figure 3. Instead or orienting toward the strongest source of chemoattractant, the agent orients itself away from the source. For some parameter settings (e.g., RA 45, SA 45) the formation or regularly spaced periodic structures is observed. The regular spacing of the structures is caused by agents attempting to move away from the source of the chemoattractant that they are depositing. The evolution of the structures is complex and highlighted in more detail in Figure 16, top row.

The circular (approximately honeycomb tiling) domains initially emerge as tight circular flows of agents. Typically a circular flow is surrounded by six weaker regions, conceptually similar to the layout of the cartridge chambers in a revolver-type pistol. The concentration of agents from the inner circle is gradually distributed to the outer chambers as the flow of agents is balanced. Over a longer time period, the stable domains begin to exert a larger influence and the regular patterning is slowly enforced (also see video recordings VR F16a). Similar behaviors are observed for the emergence of regular striped domains (Figure 16, bottom row). Initially stripes formed in a number of different directions, but one particular direction begins to predominate, transforming neighboring

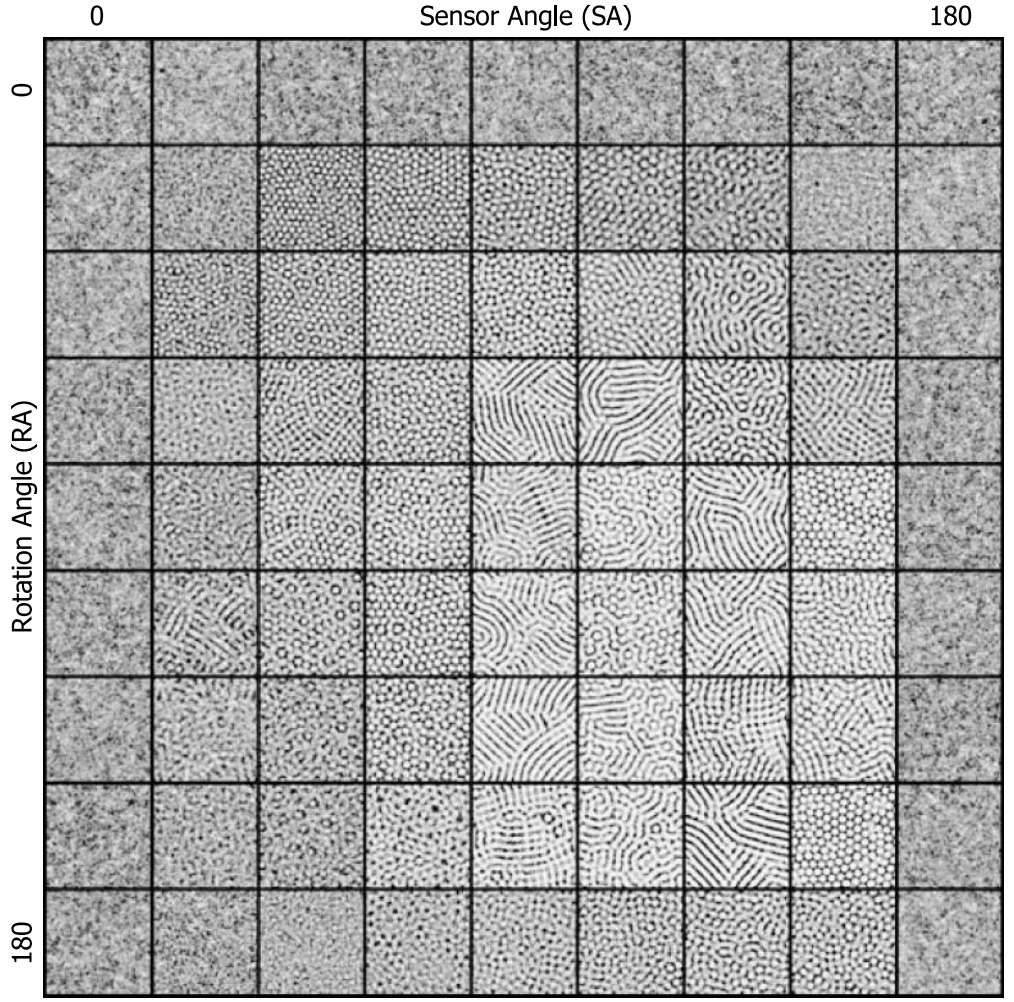

Figure 15. Patterns with chemorepulsion behaviors formed by varying SA and RA from 0 to 180 deg. 300 × 300 lattice, %p 15, SO 19, run for 500 steps. Agent trails shown.

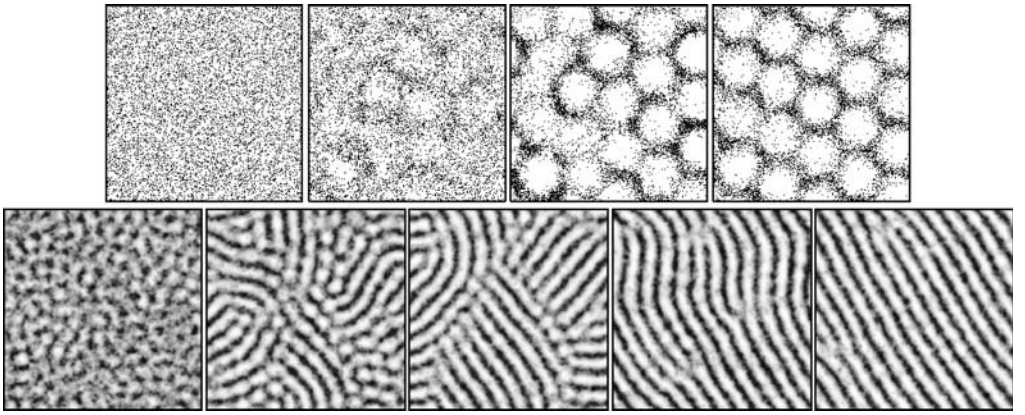

Figure 16. Evolution to regular periodic spacing in repulsive agents. Top row: 200 × 200 lattice, %p 20, RA 45, SA 45, SO 40. Individual dark flecks represent agent density. Bottom row: 200 × 200 lattice %p 20, RA 67.5, SA 112.5, SO 13. Darkness corresponds to chemoattractant values.

striped regions to the dominant orientation, and ultimately resulting in a regularly distributed striped field (VR F16b, VR F16c).

4 Pattern Formation with Pre-patterning Stimuli

Since it is possible to generate complex patterns without preexisting cues, the role of pre-patterning stimuli should be to guide or modify, in some way, the underlying pattern formation process. Results of the response to pre-patterning cues are presented below. The preexisting cues are represented by sources of chemoattractant. The exact location of the source is represented by pixel locations in the agent environment lattice. The strength of the stimulus is related to the pixel intensity of the stimulus. At each scheduler step locations that are marked by stimulus pixels were projected to the chemoattractant layer (the layer in which the agent particles deposit and sense their environment). The projection strength can be modified by specifying a *weighting* factor (stimulus value × weight) where the weight is typically within the range 0.01 to 0.1 (depending on the area of the stimulus source). The projected pre-pattern stimuli are subject to the same diffusion process that applies to the agent-produced chemical. The weighting of the pre-pattern stimuli affects both the steepness and the area of the local concentration gradient (Figure 17).

An example of the effect of simple pre-pattern stimuli is shown in Figure 18. When initialized with a small population size, the network initially emerges in much the same way as without pre-pattern cues. The network soon condenses on the strong chemotaxis stimuli presented by the two stimuli points. Using these points as an anchor, the network evolves until redundant paths are removed and the shortest path is left (VR F18). When the number of stimulus sources is increased, the network evolution exhibits minimization behavior characteristic of minimum Steiner tree formation (for a given set of points, the Steiner tree represents the shortest amount of connecting material when all points are connected). Network evolution under the influence of pre-pattern stimuli appears to exhibit quasi-physical surface tension effects. This is an emergent phenomenon, which is clearly not specified by the particle algorithm (given in Figure 3). The surface tension effects resemble those seen in soap films and appear to follow Plateau's laws (meeting paths preferentially connect at three-way nodes and with 120-deg angles). In fact the network evolution around pre-patterning stimuli appears to correspond well with recent experimental network evolution using lipid nanotubes [31]. The final Steiner tree is formed when redundant network paths are shortened and closed by the emergent surface tension effects (Figure 19). The video recordings in VR F19 illustrate that the network converges on the final tree shape, despite often following very different dynamic graph trajectories.

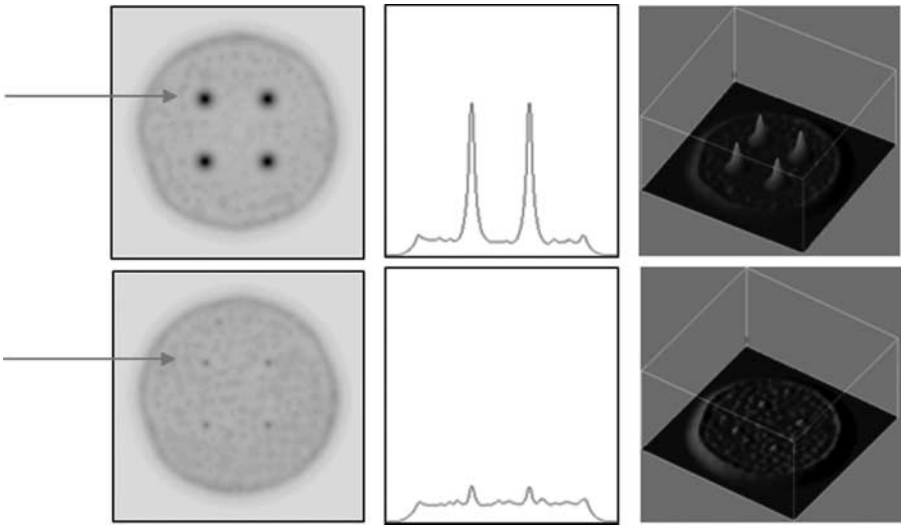

Figure 17. Visualization of the effect of pre-patterning stimuli and the effect of stimuli weighting. Left to right: Chemoattractant levels of a circular sheet of agents with pre-pattern stimuli cues arranged as the four corners of a square; cross-section plot (indicated by arrow); 3D interpretation of left image. Pre-pattern projection weighting: top row, 0.06, bottom row, 0.01.

4.1 Effect of Modifying Pre-pattern Stimuli Weights

The small agent population sizes used in the above examples can result in instances where cycles cannot be closed due to the arrangement of the stimulus points. This may be desirable when the patterning aim is to maintain branching connectivity (for example, in vascular or alveolar connectivity). By reducing the weight of the pre-pattern stimuli, the stimulus nodes exert less of an influence on the agent particles, due to the smaller gradients and reduced area of influence. Subsequently the network is less restricted in its evolution. Figure 20 (VR F20) shows a network whose evolution has been stopped by a particular ringlike configuration of points. The arrangement of stimulus points (top row, far right) coincides with the shape of the cyclic area, and the contraction of the cycle does

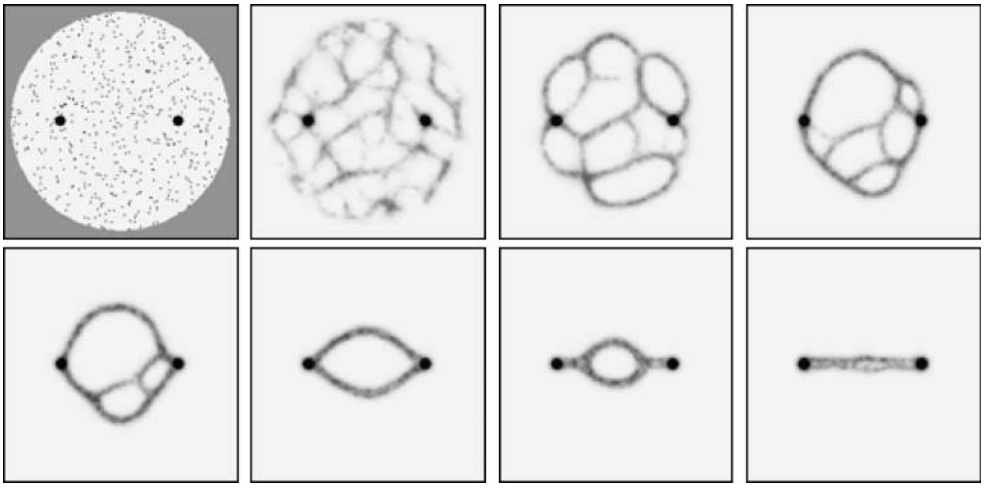

Figure 18. Pattern formation and evolution under the influence of pre-patterning cues. 200 × 200 lattice, %p 2, RA 45, SA 45, SO 9. Pre-pattern projection weighting: 0.01. Top left: Environment shows pre-pattern cues (dark spots), initial agent positions (small gray flecks), and boundary of the environment (uniform gray). Remaining images (left to right): Evolution of network formation (agent trails shown) as the network becomes "snagged." Minimization of the network continues until the shortest path between the stimuli remains.

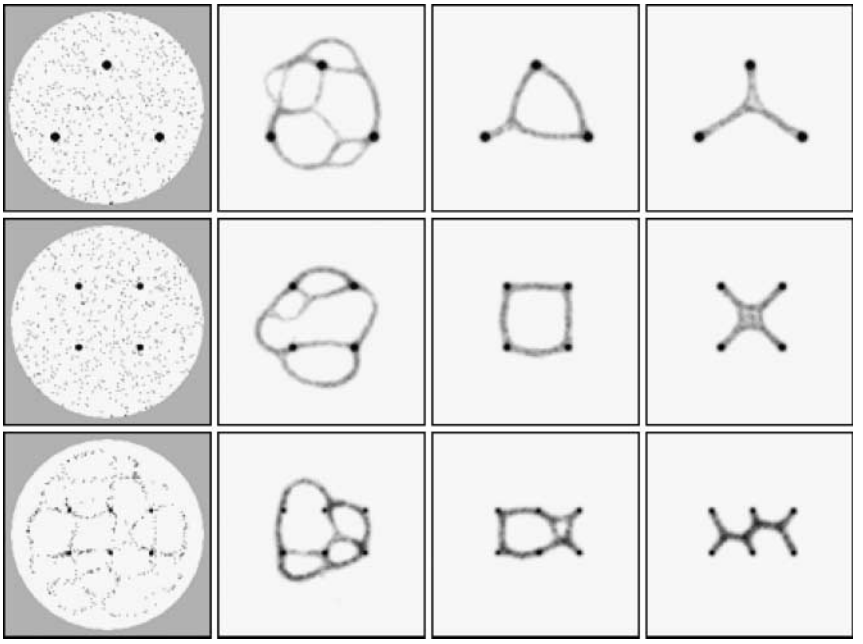

Figure 19. Approximation of Steiner minimum trees by evolving network in response to regular pre-pattern cues. Lattice 200 × 200, RA 45, SA 45, SO 9, %p 2 (except bottom row, %p 1.25). Pre-pattern projection weighting: 0.01. Left: agent particle positions. Remaining columns: chemoattractant pre-pattern stimuli and trail patterns.

not complete, because the attraction of the stimuli cancels out the contraction force. By reducing the weighting of the pre-pattern stimuli, their influence is reduced and the cycle is closed. The effect of the weight reduction appears to be a *loosening* of the tension in the network. The enclosed shape (bottom row, middle picture) shows a minimal area enclosing all of the points. By randomly removing agents from the environment it is possible to mimic, in a very simple way, the effects of cellular apoptosis. The network dynamically responds to a reduction in the number of its constituent parts by maintaining minimal connections to the pre-pattern nodes. Finally, strongly increasing the weighting

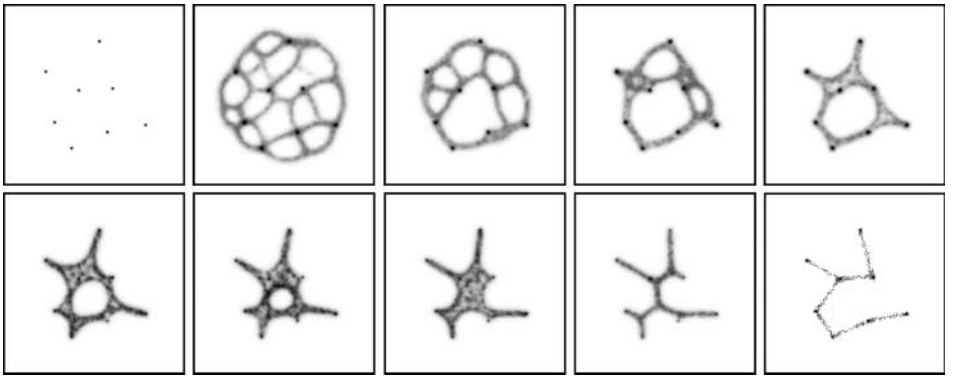

Figure 20. Effects of reducing and increasing pre-pattern stimuli weights. Lattice 200 × 200, RA 45, SA 45, %p 5 (2000 agents), SO 9. Pre-pattern weighting: 0.05. Trail patterns shown. Top row, 1–5: Condensation of pattern around points. Cyclic layout of points prevents closure (5). Bottom row, 6–10: Reducing stimulus strength to 0.01 allows closure (6–8). Randomly removing agents shrinks pattern (~600 agents remaining). 9: Increase of pre-pattern stimulus strength to 0.5 (tightening) removes Steiner nodes, forming the minimum spanning tree (10). Note that the final image shows agent particle positions, due to the large difference between pre-pattern concentration and trail concentration.

of the pre-pattern nodes has the effect of *tightening* the network (bottom row, far right). The agents are much more strongly influenced by the pre-pattern stimuli, and the network nodes approximating Steiner points are removed, the network forming the minimum spanning tree structure (bottom row, final image; the agent positions are indicated, as the chemical trails cannot be directly visualized due to the difference in strength of the stimulus and network trail values).

4.2 Deformation of Pre-existing Sheet Structure by Plasmodial Shrinkage

The previous example shows that as the number of pre-pattern stimuli increases, there is an increased likelihood that the network connectivity will be affected by initial configuration of the agents. Cyclic areas are less likely to be closed, and the network maintains high connectivity at the expense of network overall length. Instead of seeding and condensing a network around the stimulus points, it is possible to use the stimuli to deform a pre-existing sheet of cells, such as those formed in Figure 9. The approach used is an approximation of the behavior of the *Physarum* plasmodium, which, after initial coverage of the environment, shrinks to form networks of transport veins connecting the food sources. The plasmodial shrinkage method populates the environment with a very large number of agent particles (%p = 50 in a 300 × 300 lattice: 45,000 agents) to ensure that the network forms a solid sheet structure. As the experiment progresses, agent particles, chosen at random, are removed from the environment. Agents are never readmitted to the environment once removed. The probability of agent removal was set to 0.00025 for each agent at every scheduler step. At early stages of the experiment (when the population was high), the number of agents removed is relatively high. As the population size decreased, so did the number of agents removed.

The results shown in Figure 21 compare the filamentous condensation approach (with low %p = 5) with the plasmodial shrinkage approach. The middle row shows three separate results from the condensation approach. The network patterns are similar despite following very different dynamic evolution

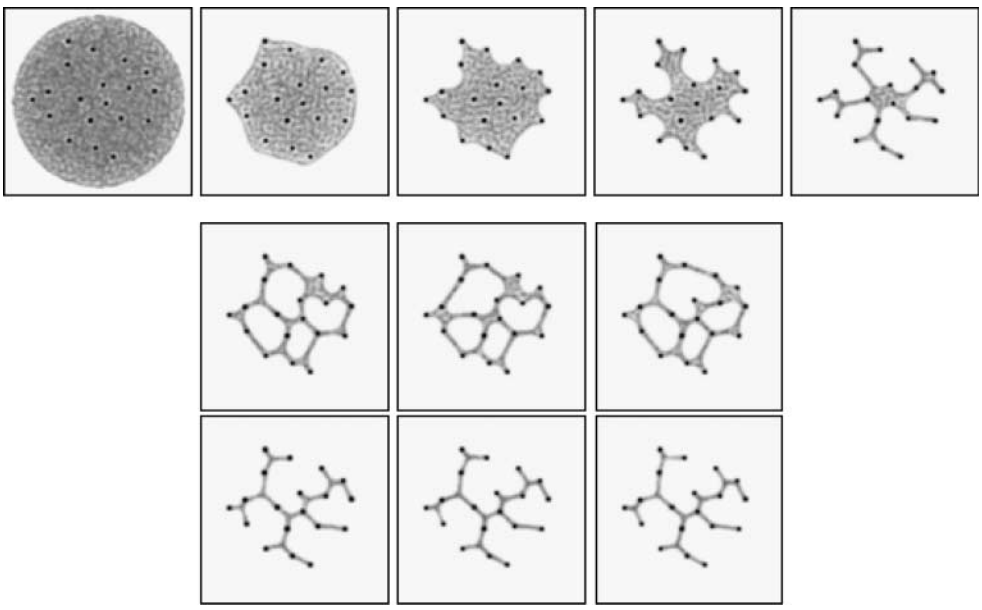

Figure 21. Use of plasmodial sheet deformation method provides identical convergence and more regular results. Lattice 300 × 300, RA 45, SA 45, SO 9, %p 5 (condensation method), %p 50 (plasmodial shrinkage method). Trail patterns shown. Top row: Evolution of one run of the sheet deformation method—the network automatically responds and adapts to a reduction in constituent parts. Middle row: Three separate results from network condensation methods—differences are seen in network structure. Bottom row: Three separate results from sheet deformation method—network structure is identical.

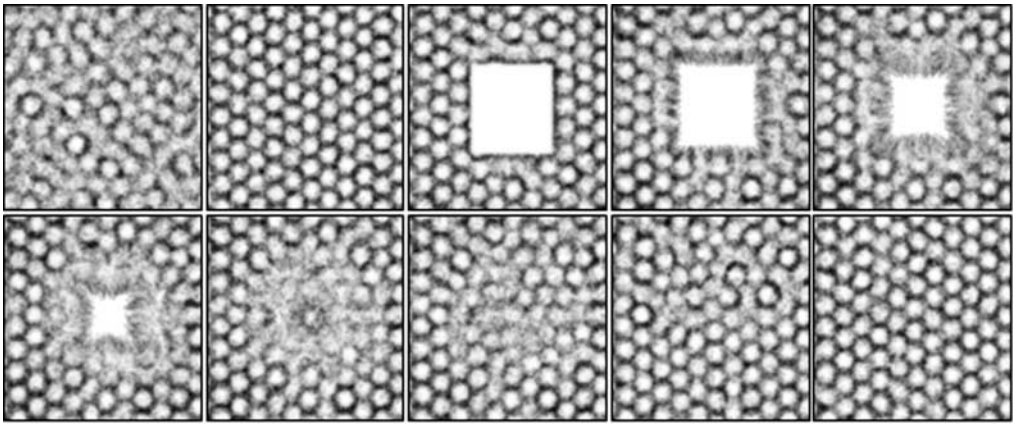

Figure 22. Damage to uniform pattern is repaired to regenerate original pattern in chemorepulsion-based patterning. Lattice 300 × 300, RA 45, SA 45, SO 27, %p 10. Trail patterns shown. Top row: initial pattern formation, regular hexagonal pattern, damage to central area, and migration of agents toward the wound area (50, 2650, 2800, 2950, 3000 steps). Bottom row: Completion of migration closes the damaged area (1–2): Reorganization of the wound area reestablishes the initial pattern (3050, 3075, 3100, 3200, 3350 steps).

trajectories (see recording VR F21a). There are differences in the network structure, however, notably toward the left side and the middle parts of the networks. The top row shows snapshots from the evolution of the plasmodial shrinkage approach. As the agent particles are randomly removed, the sheet dynamically deforms and reconfigures itself, influenced by the strong gradients of the pre-pattern stimuli (corresponding to *Physarum* food sources). The relatively slow rate of particle removal ensures that the number of agents in the sheet is uniformly distributed and that particle flux can adapt in time to the changing environment. Faster rates of removal result in the spontaneous formation of cyclic areas—the sheet deformation is unbalanced, resulting in a *tearing* of the sheet and holes being formed. The sheet maintains a minimal area as it shrinks, and the final results (bottom row, from three separate experiments) show identical network configurations. Further examination of the dynamic evolution of the plasmodial sheet for each separate experiment (VR F21b,c,d) shows an identical evolution pattern.

4.3 Pattern Repair in Response to External Damage

The previous examples of pre-patterning stimuli use the cues to guide the patterning process. The automatic reconfiguration of the network in response to a gradual removal of network components suggests methods to investigate how pattern formation mechanisms adapt to changes in their environment. Most investigations into pattern formation concentrate on the initial pattern formation process where structure is built from the constituent parts (for example, during embryogenesis) and regular stable patterns are formed. The gradual removal of agent particles resembles apoptotic reshaping of initial patterning. Other mechanisms that affect patterning are not as gentle as apoptotic re-patterning—many pattern formation processes also occur in the repair of damage to bodily structures, for example in wound healing. Experiments were carried out to assess the effect of damage to the established patterns formed by chemorepulsion- and chemoattraction-based patterning. A synthetic wound was created by the instantaneous removal of agents within a square region. The agents that were removed were replaced at random locations in the undamaged area to maintain the same population size. During the agent replacement period no agents were allowed to cross the wound boundary. When the number of agents was the same as before the damage was inflicted, the agents were allowed to migrate into the wound area. Figure 22 shows the behavior of chemorepulsion agents during the initial patterning process and in response to damage infliction. The figure shows the uniform flux of agents into the wound area and the closure of the wound. The initial pattern is reestablished under the influence of the undamaged areas surrounding the wound site. The final healed pattern is identical to the pattern before the damage was inflicted (VR F22).

The same approach was used to investigate the response of chemoattraction-based agents to damage (Figure 23). A population of agents was used to generate an initial dynamic reticular pattern before the square wound area was inflicted. The agents removed from the damaged area were seeded at random positions outside the damaged area to maintain the same number of particles. The agents were then allowed access to the wound area. However, instead of the uniform flux of agents into the wound area shown by the chemorepulsion approach, the agents began a gradual insertion of branchlike processes into the wound margin. The interaction between distant processes gradually spanned the wound area, and the area was then covered by branching from this initial connectivity. The reticular pattern was reestablished, but the patterning was different from the initial configuration before the damage was inflicted (VR F23).

5 Conclusions and Scope for Further Work

We have presented a particle-based approach to complex pattern formation and evolution by emergent transport networks inspired by the behaviors of *Physarum polycephalum*—an organism whose very existence is based on mobile pattern formation and pattern evolution. The results presented in this article are in the spirit of chemotaxis-based cell migration approaches to pattern formation. Unlike previous approaches, however, the patterns formed by this approach are composed of dynamic particle flux. This particle-based approach utilizes extremely simple behaviors based on movement influenced by a forward sensory bias and simple chemotaxis (chemoattraction and chemorepulsion). The local activation mechanism is generated by the migration of agent particles toward (or away from) local gradients of chemoattraction. The diffusion mechanism is based upon simple diffusion of chemoattractant, whose depletion affects the region of sensory influence of the agent particles.

By modifying the sensory parameters a wide variety of chemoattraction-based complex patterning was observed, including spotted, striped, labyrinthine, and reticular patterns. The patterns also exhibited sensitivity to both diffusion (affecting aggregation strength) and population size (affecting patterning by diminished local activation at small %p, and reduced movement at high %p). The scale of the pattern formation processes (size, network path width, and granularity) was also affected by the sensory coupling distance of each agent.

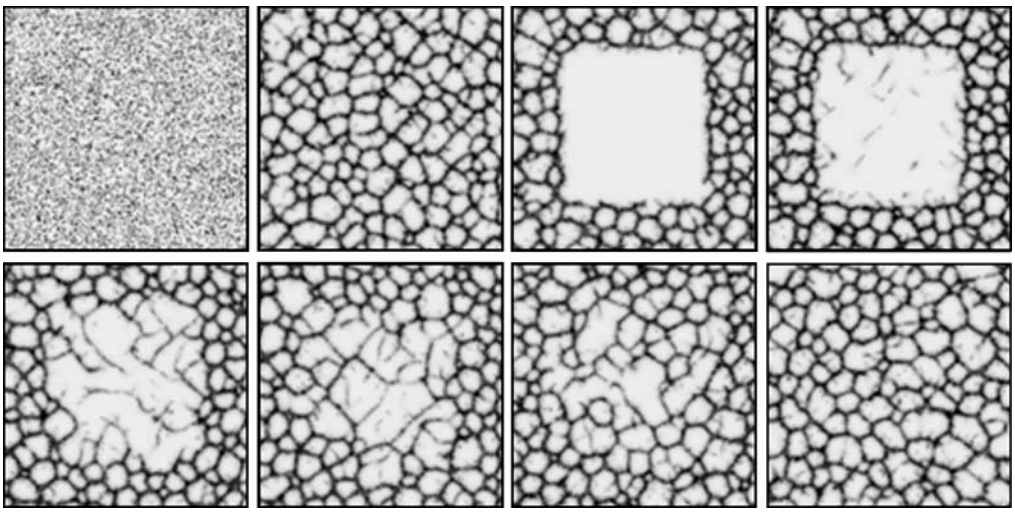

Figure 23. Damage to reticular network is repaired by chemoattraction-based patterning. Lattice 300 × 300, RA 45, SA 22.5, SO 3, %p 10. Trail patterns shown. Top row: initial pattern formation, reticular network, damage to central area, and insertion of network processes into the wound area (0, 350, 840, 980 steps). Bottom row: Network processes gradually span the damaged area and branching structures emerge to cover the damaged area (1680, 3150, 4900, 12600 steps).

The flux of agents corresponded to the characteristic shuttle streaming movement seen in *Physarum* gel-sol interactions. The complexity of the emergent patterning was due to the patterns actually being composed of the flux of agent particles—even apparently stable patterns were composed of the flux of highly mobile components. The dynamic nature of the pattern formation process resulted in complex quasimechanical emergent behaviors in the patterning. These behaviors were characterized by bifurcation of network patterns in response to random instabilities in network path flux, coupled with the merging of network flows, generating highly dynamic network patterns. Another characteristic pattern was the closure of cyclic network structures by an apparent tension mechanism (caused by the local increase in network flux when following shorter paths). The movement of particles altered the structure of the network, in turn affecting the movement of agents in a complex cycle of interactions.

Using an approach based on chemorepulsion, characteristic Turing-like dissipative patterns of regular spotted and striped arrays were generated. These patterns also exhibited complex evolution—areas of initial patterning propagated to nearby areas in competition with other local patterns. Ultimately, one particular area of patterning predominated and covered the entire area with a regular (although dynamic) pattern.

The complex pattern formation was coupled to preexisting pattern stimuli, and network minimization behaviors were observed when the particle population condensed in networks surrounding the stimuli points. Similar network configurations converged from very different initial distributions. By adjusting the strength of the pre-pattern stimuli (*tightening* and *loosening*), the network configuration was changed from a Steiner tree approximation to a minimum spanning tree approximation. By utilizing a large population of particles a synthetic plasmodium-like sheet was generated, which automatically reconfigured itself in response to removal of its components—resulting in repeatable network minimization.

Finally, examples of how the pattern formation mechanisms responded to damage to the patterns were demonstrated. Although mechanically and chemically very simple in comparison with the complex cascade of interactions in in-vivo wound healing, it was shown that chemorepulsion-based behaviors were able to repair damage by a closing of the wound area and reestablish the original patterning. Chemoattraction-based patterns were able to repair the damaged areas by interdigitating migration into the wound area, gradually reestablishing the network, although without recovering the original pattern.

With respect to biological pattern formation, the results show that complex patterning can be achieved using a cell migration approach and only a single chemoattractant chemical. The recent demonstration that human umbilical vein endothelial cells can spontaneously self-assemble into complex vascular network patterns when placed on a nutrient substrate provides experimental support for the role of chemotaxis in in-vivo pattern formation [42]. Another biologically useful property of the agent-based pattern formation is the functional properties of the pattern mechanisms—the patterns reflect desirable physical properties such as high connectivity in reticular patterns (which is essential in vascular networks to ensure adequate perfusion to body tissues) and minimal path costs shown in the evolved contracting patterns (which is essential for efficient transport of nutrients). The emergent functionality is as a result of the quasi-physical influences on the network evolution. The geometry of the pre-pattern cues (for example, the distances and angles between the stimulus points) affects the network evolution indirectly in more subtle ways than simple metrics of distance or angle might initially suggest.

Further work could be carried out to extend the pattern formation process into three dimensions to assess the quality and the quasi-physical properties of patterning. It should also be noted that the very simple sensory and movement behaviors of the agents described herein occupy only a tiny subset of possible agent morphologies and behaviors. It would be very surprising if the patterns formed with other agent morphologies and behaviors did not prove as complex as those described here. These results were inspired by the behaviors of *Physarum*, stimulated by recent research using the organism as an unconventional computing substrate. We have shown that is possible to use *Physarum*-like pattern formation and evolution to provide solutions to computational problems whose problem definition and solution may be represented as spatial patterns. *Physarum* has a number of advantages over other unconventional computing substrates: it is inexpensive, fault tolerant, and relatively simple to culture and observe. Its only disadvantages are that it is often rather unpredictable and difficult to control, and has slow growth and movement (compared to classical computing devices). We suggest that it might

be possible to develop synthetic materials, using simple chemotaxis and migration such as described here, which would overcome some of the few limitations of using the real organism.

Acknowledgments

The author acknowledges the support of the Leverhulme Trust for a research fellowship under the project: F/00577/1 "Mould Intelligence—Designing Biological Amorphous Robots" (principal investigator Andrew Adamatzky).

References

1. Adamatzky, A. (1991). Neural algorithm for constructing minimum spanning tree of a finite planar set. *Neural Networks World*, *6*, 335–339.
2. Adamatzky, A. (2007). *Physarum* machine: Implementation of a Kolmogorov-Uspensky machine on a biological substrate. *Parallel Processing Letters*, *17*(4), 455–467.
3. Adamatzky, A. (2008). Growing spanning trees in plasmodium machines. *Kybernetes*, *37*(2), 258–264.
4. Adamatzky, A., & Jones, J. (2008). Towards *Physarum* robots: Computing and manipulating on water surface. *Journal of Bionic Engineering*, *5*(4), 348–357.
5. Adamatzky, A., & Jones, J. (2009). Programmable reconfiguration of *Physarum* machines. *Natural Computing,* DOI: 10.1007/s11047-009-9146-8.
6. Aono, M., & Hara, M. (2007). Amoeba-based nonequilibrium neurocomputer utilizing fluctuations and instability. In *Lecture notes in computer science*, vol. 4618, p. 41.
7. Bebber, D., Hynes, J., Darrah, P., Boddy, L., & Fricker, M. (2007). Biological solutions to transport network design. *Proceedings of the Royal Society B: Biological Sciences*, *274*(1623), 2307–2315.
8. Ben-Jacob, E. (2003). Bacterial self-organization: Co-enhancement of complexification and adaptability in a dynamic environment. *Philosophical Transactions: Mathematical, Physical and Engineering Sciences*, *361*(1807), 1283–1312.
9. Bizon, C., Shattuck, M., Swift, J., McCormick, W., & Swinney, H. (1998). Patterns in 3D vertically oscillated granular layers: Simulation and experiment. *Physical Review Letters*, *80*(1), 57–60.
10. Bonabeau, E. (1997). From classical models of morphogenesis to agent-based models of pattern formation. *Artificial Life*, *3*(3), 191–211.
11. Bonabeau, E. (1998). A model for the emergence of pillars, walls and royal chambers in termite nests. *Philosophical Transactions: Biological Sciences*, *353*(1375), 1561–1576.
12. Bonabeau, E. (2002). Agent-based modeling: Methods and techniques for simulating human systems. *Proceedings of the National Academy of Sciences of the U.S.A.*, *99*(3), 7280–7287.
13. Burstedde, C., Klauck, K., Schadschneider, A., & Zittartz, J. (2001). Simulation of pedestrian dynamics using a two-dimensional cellular automaton. *Physica A: Statistical Mechanics and its Applications*, *295*(3–4), 507–525.
14. De Kepper, P., Boissonade, J., & Epstein, I. (1990). Chlorite-iodide reaction: A versatile system for the study of nonlinear dynamic behavior. *The Journal of Physical Chemistry*, *94*(17), 6525–6536.
15. Deneubourg, J., Aron, S., Goss, S., & Pasteels, J. (1990). The self-organizing exploratory pattern of the Argentine ant. *Journal of Insect Behavior*, *3*(2), 159–168.
16. Dorigo, M., Bonabeau, E., & Theraulaz, G. (2000). Ant algorithms and stigmergy. *Future Generation Computer Systems*, *16*(8), 851–871.
17. Dorigo, M., & Gambardella, L. M. (1997). Ant colonies for the travelling salesman problem. *BioSystems*, *43*(2), 73–81.
18. Gierer, A., & Meinhardt, H. (1972). A theory of biological pattern formation. *Biological Cybernetics*, *12*(1), 30–39.
19. Gunji, Y. P., Shirakawa, T., Niizato, T., & Haruna, T. (2008). Minimal model of a cell connecting amoebic motion and adaptive transport networks. *Journal of Theoretical Biology*, *253*(4), 659–667.
20. Helbing, D. (2001). Traffic and related self-driven many-particle systems. *Reviews of Modern Physics*, *73*(4), 1067–1141.

21. Hickey, D., & Noriega, L. (2008). Relationship between structure and information processing in *Physarum polycephalum*. *International Journal of Modelling, Identification and Control*, *4*(4), 348–356.

22. Ishiguro, A., Shimizu, M., & Kawakatsu, T. (2006). A modular robot that exhibits amoebic locomotion. *Robotics and Autonomous Systems*, *54*, 641–650.

23. Jarrett, T., Ashton, D., Fricker, M., & Johnson, N. (2006). Interplay between function and structure in complex networks. *Physical Review E*, *74*(2), 26116.

24. Jones, J. (2010). The emergence and dynamical evolution of complex transport networks from simple low-level behaviours. *International Journal of Unconventional Computing*, *6*(2), 125–144.

25. Jones, J. (2008). An emergent pattern formation approach to dynamic spatial problems via quantitative front propagation and particle chemotaxis. *International Journal of Unconventional Computing*, *4*(4), 1–34.

26. Jones, J. (2009). Passive vs active approaches in particle approximations of reaction-diffusion computing. *International Journal of Nanotechnology and Molecular Computation*, *1*(3), 37–63.

27. Kessler, M., & Werner, B. (2003). Self-organization of sorted patterned ground. *Science*, *299*(5605), 380–383.

28. Koch, A., & Meinhardt, H. (1994). Biological pattern formation: From basic mechanisms to complex structures. *Reviews of Modern Physics*, *66*(4), 1481–1507.

29. Liaw, S., Yang, C., Liu, R., & Hong, J. (2001). Turing model for the patterns of lady beetles. *Physical Review E*, *64*(4), 41909.

30. Liu, R., Liaw, S., & Maini, P. (2006). Two-stage Turing model for generating pigment patterns on the leopard and the jaguar. *Physical Review E*, *74*(1), 11914.

31. Lobovkina, T., Dommersnes, P. G., Tiourine, S., Joanny, J. F., & Orwar, O. (2008). Shape optimization in lipid nanotube networks. *The European Physical Journal E—Soft Matter*, *26*(3), 295–300.

32. Manoussaki, D. (2003). A mechanochemical model of angiogenesis and vasculogenesis. *Mathematical Modelling and Numerical Analysis*, *37*(4), 581–599.

33. Merks, R., & Glazier, J. (2006). Dynamic mechanisms of blood vessel growth. *Nonlinearity*, *19*(1), 1–10.

34. Morriss-Kay, G., & Sokolova, N. (1996). Embryonic development and pattern formation. *The FASEB Journal*, *10*(9), 961–968.

35. Murray, J. (1988). How the leopard gets its spots. *Scientific American*, *258*(3), 80–87.

36. Murray, J., & Oster, G. (1984). Cell traction models for generating pattern and form in morphogenesis. *Journal of Mathematical Biology*, *19*(3), 265–279.

37. Nakagaki, T., Yamada, H., & Hara, M. (2004). Smart network solutions in an amoeboid organism. *Biophysical Chemistry*, *107*(1), 1–5.

38. Nakagaki, T., Yamada, H., & Toth, A. (2000). Maze-solving by an amoeboid organism. *Nature*, *407*, 470.

39. Oster, G. (1988). Lateral inhibition models of developmental processes. *Mathematical Biosciences*, *90*, 265–286.

40. Ouyang, Q., & Swinney, H. (1991). Transition from a uniform state to hexagonal and striped Turing patterns. *Nature*, *352*(6336), 610–612.

41. Reynolds, C. (1987). Flocks, herds and schools: A distributed behavioral model. *ACM SIGGRAPH Computer Graphics*, *21*(4), 25–34.

42. Serini, G., Ambrosi, D., Giraudo, E., Gamba, A., Preziosi, L., & Bussolino, F. (2003). Modeling the early stages of vascular network assembly. *The EMBO Journal*, *22*, 1771–1779.

43. Shirakawa, T., Adamatzky, A., Gunji, Y., & Miyake, Y. (in press). On simultaneous construction of Voronoi diagram and Delaunay triangulation by *Physarum polycephalum*. *International Journal of Bifurcation and Chaos*.

44. Takagi, S., & Ueda, T. (2007). Emergence and transitions of dynamic patterns of thickness oscillation of the plasmodium of the true slime mold *Physarum polycephalum*. *Physica D: Nonlinear Phenomena*, *237*(3), 420–427.

45. Takamatsu, A. (2006). Spontaneous switching among multiple spatio-temporal patterns in three-oscillator systems constructed with oscillatory cells of true slime mold. *Physica D: Nonlinear Phenomena*, *223*(2), 180–188.

46. Takamatsu, A., Takaba, E., & Takizawa, G. (2009). Environment-dependent morphology in plasmodium of true slime mold *Physarum polycephalum* and a network growth model. *Journal of Theoretical Biology*, *256*(1), 29–44.

47. Tero, A., Kobayashi, R., & Nakagaki, T. (2007). A mathematical model for adaptive transport network in path finding by true slime mold. *Journal of Theoretical Biology*, *244*(4), 553–564.

48. Tosin, A., Ambrosi, D., & Preziosi, L. (2006). Mechanics and chemotaxis in the morphogenesis of vascular networks. *Bulletin of Mathematical Biology*, *68*(7), 1819–1836.

49. Tsuda, S., Aono, M., & Gunji, Y. (2004). Robust and emergent *Physarum* logical-computing. *BioSystems*, *73*(1), 45–55.

50. Tsuda, S., Zauner, K., & Gunji, Y. (2007). Robot control with biological cells. *BioSystems*, *87*(2–3), 215–223.

51. Turing, A. (1952). The chemical basis of morphogenesis. *Philosophical Transactions of the Royal Society of London. Series B, Biological Sciences (1934–1990)*, *237*(641), 37–72.

52. Turk, G. (1991). Generating textures on arbitrary surfaces using reaction-diffusion. In *Proceedings of the 18th Annual Conference on Computer Graphics and Interactive Techniques*. New York: ACM.

53. Tyson, J., Alexander, K., Manoranjan, V., & Murray, J. (1989). Spiral waves of cyclic AMP in a model of slime mold aggregation. *Physica D: Nonlinear Phenomena*, *34*(1–2), 193–207.